

Sensors on Textile Fibres Based on Ag/a-C:H:O Nanocomposite Coatings^{*}

Regular Paper

Martin Drabik^{1,*}, Nina Vogel-Schäuble²,
Manfred Heuberger¹, Dirk Hegemann¹ and Hynek Biederman³¹ Empa, Swiss Federal Laboratories for Materials Science and Technology, St. Gallen, Switzerland² Empa, Swiss Federal Laboratories for Materials Science and Technology, Dübendorf, Switzerland³ Charles University in Prague, Faculty of Mathematics and Physics, Department of Macromolecular Physics, Prague, Czech Republic* Corresponding author E-mail: martin.drabik@empa.ch

Received 3 December 2012; Accepted 4 March 2013

© 2013 Drabik et al.; licensee InTech. This is an open access article distributed under the terms of the Creative Commons Attribution License (<http://creativecommons.org/licenses/by/3.0>), which permits unrestricted use, distribution, and reproduction in any medium, provided the original work is properly cited.

* An early version of this paper has been presented at The International Conference on Nanomaterials: Fundamentals and Applications - NFA2012, Slovakia

Abstract In this contribution we present a study of the vacuum deposition process of metal/plasma polymer nanocomposite thin films monitored using plasma diagnostics (optical emission spectroscopy). We investigate the electrical properties of the nanocomposite structures suitable for their application as humidity sensors. Furthermore, the film microstructure is characterized by transmission electron microscopy and electron diffraction analysis. The amount of silver in the nanocomposite is evaluated using inductively coupled plasma optical emission spectrometry and the morphology of the structured system of metal electrodes and nanocomposite films on monofilament textile fibres is visualized using scanning electron microscopy. Ageing of nanocomposite coatings and the influence of an aqueous environment on their internal structure and properties are discussed.

Keywords Nanocomposite Thin Film, Sensor, Textile Fibre

1. Introduction

Humidity sensors are nowadays utilized in many different industrial applications (semiconductors industry, pharmaceuticals, etc.), the electronic control of environmental conditions, medical fields (sterilizers, incubators, etc.) agriculture (green house air-conditioning) and far more [1]. Common methods used for the measurement of humidity are indirect, i.e., the humidity is inferred from its effect on the material, rather than measured directly. Conjugated conductive polymers are a common class of materials used for humidity sensing; others include resistive ceramics, dielectric polymers or resistive polyelectrolytes [2]. Their working principle is often based on porous thin films, on which water vapour condensates so that their physical properties change. Two fundamental categories of polymer humidity sensors are recognized according to their sensing mechanism: resistive (responds to water by changes in conductivity) and capacitive (changes in dielectric constant) types [3]. The advantages of polymer sensors mainly include resistance to contamination and

low cost, while common disadvantages include limited long-term stability and limited operating temperature range, as well as slower response time and hysteresis [2].

Functional textiles and clothes have received growing attention from several research institutes worldwide. Over the past decade, nano- and micro-technologies have created an additional momentum in textile research [4]. A sensitive textile fibre (textile-electronic-fibre or e-fibre) is the first step to integrating electronic elements into fabrics and further design and manufacture sensing and acting textiles for utilization in medical, sports or home environments. This concept includes, for example, on-body sensor components capable of monitoring the biometric status of the wearer continuously.

A promising group of materials in this field is nanocomposites. In particular, metal/plasma polymer nanocomposite coatings are interesting due to a wide range of possible applications as a result of great freedom in tuning their mechanical, electrical and optical properties according to the special requirements of any particular application [5-7]. These nanocomposite films have already been identified as a suitable type of material for sensor applications [8].

The filling factor (or volume fraction ratio) f is the principal parameter describing the structure of a nanocomposite coating (even composites of metal oxides [9]). It is defined as the volume of metal inclusions in the total volume of the composite material:

$$f = \frac{V_{\text{metal}}}{V_{\text{composite}}} \quad (1)$$

The structure of such a nanocomposite film (size, shape and spatial distribution of the metal nanoparticles dispersed in the insulating plasma polymer matrix), among others, also determines its electrical properties [10, 11]. Composites with a low amount of metal inclusions are electrically insulating due to their large inter-particle separation. On the other hand, when the filling factor is high enough, particles start to contact each other and form electrically an interconnected network (metallic structure). The conductivity of such material increases non-linearly, although it might still be orders of magnitude below the bulk conductivity of a solid state metal. The value of the filling factor f_c , at which the structure of a nanocomposite film switches from an insulating to a conductive nature, is commonly known as the percolation threshold. The conductivity of nanocomposite coatings might easily increase by 10 orders of magnitude in this region of filling factor values, depending on the nature of materials [12, 13]. Detection of any changes in the electrical properties of such nanocomposites is readily available and their utilization in sensor applications is at hand.

Several plasma-based deposition techniques have been explored in order to incorporate metal nanoparticles into a plasma polymer matrix, e.g., simultaneous magnetron sputtering from metal and polymer targets or metal evaporation during plasma-enhanced chemical vapour deposition (PECVD) [14-16]. Plasma technology offers a controlled film growth while maintaining a high surface diffusion at low substrate temperatures. The deposition of metallic coatings onto textile fibres (i.e., metallization) has already been industrially established [17, 18]. However, the deposition of nanocomposite coatings is not yet industrialized, due to factors like too low deposition rates and restrictions in the deposition area. Also, different applications of such e-fibre sensors (e.g., for sensing strain or relative humidity) require different combinations of nanoparticle, polymer and electrode materials and therefore an individual approach is needed. For sensing, a change in resistivity can readily be recorded near the percolation threshold, e.g., when humidity is entering the plasma polymer matrix of the nanocomposite or due to the application of an external force. Furthermore, as a novel approach, chemical changes in the metal-containing layer can lead to metal ion release in aqueous environments.

In this contribution, we present a study of the vacuum deposition process using plasma diagnostics (optical emission spectroscopy [OES]) and assess the structural properties of metal/plasma polymer nanocomposite structures relevant to their application as sensors. In particular, the characterization of film microstructure by transmission electron microscopy (TEM), electron diffraction analysis and inductively coupled plasma optical emission spectrometry (ICP-OES) and the electrical properties of the films are described. Ageing of such thin films and the influence of an aqueous environment on their structure and properties is also discussed.

2. Experimental

2.1 Deposition method

The combination of plasma polymerization (PECVD) of ethene and simultaneous sputtering of a silver target was chosen as the deposition method for the preparation of nanocomposite coatings where silver particles are embedded in an oxidized amorphous hydrocarbon plasma polymer matrix (Ag/a-C:H:O) [19]. A low-pressure plane-parallel capacitively coupled plasma reactor was used with a top Ag electrode connected to an RF power source (13.56 MHz) (see Figure 1). All substrates were placed on the grounded bottom electrode at a distance of 5cm. Working gas composed of Ar (sputter gas), CO₂ (reactive gas) and C₂H₄ (monomer gas) was introduced into the chamber through a gas shower in the top plate of the reactor. The gas composition was

controlled via the flow rate of the respective gas at 50/6/1sccm, respectively. The working gas pressure was held constant at 5Pa. The main experimental parameter was the RF discharge power. It varied between 20W and 150W, which allowed us to obtain nanocomposite films with various filling factors.

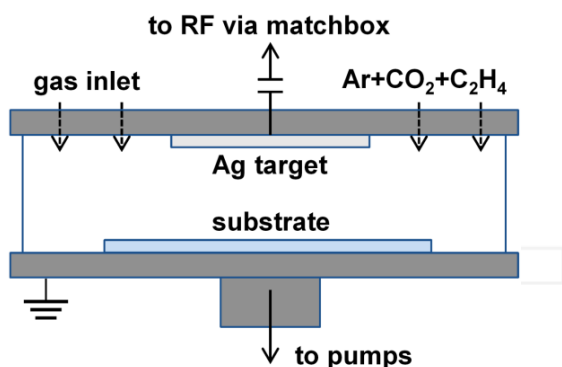


Figure 1. Schematic drawing of vacuum deposition chamber.

2.2 Characterization techniques

The composition and stability of the glow plasma discharge was monitored *in-situ* during the deposition process by optical emission spectroscopy (OES) using an AvaSpec-ULS2048-USB2 spectrometer (Avantes, Netherlands) connected to the chamber through an optical fibre. The spectra were recorded over a wavelength range of 300–820nm. The obtained spectra were analysed using the atomic spectra database provided by the National Institute of Standards and Technology [20] and individual literature sources [21].

The filling factor of the nanocomposite thin films was estimated by inductively coupled plasma optical emission spectrometry (ICP-OES) using Optima 3000 (Perkin Elmer, USA). For this post-analysis, the films deposited on glass slides (Assistent, Germany) were dissolved in 2ml concentrated nitric acid and diluted with 8ml water up to 10ml. The solution was then injected into the spectrometer and optically analysed (Ag lines at 328.068nm and 338.289nm). The calibration was performed using an independent Ag standard solution of 1mg·ml⁻¹.

The microstructure of the nanocomposite films deposited on carbon foils on Cu grids S160 (Plano, Germany) was characterized by a high resolution transmission electron microscope (HR-TEM) JEM-2200FS (Jeol, Japan) operating at 200kV. The obtained micrographs were analysed for the size and shape of the silver nanoparticles in order to obtain the statistical distributions. The crystal structure of the formed nanoparticles was obtained using electron diffraction patterns by selected-area diffraction (SAD) analysis and evaluated according to the database provided by the International Centre for Diffraction Data [22]. The obtained digital TEM photographs were

corrected for contrast and/or brightness where necessary. The images were then statistically processed by ImageJ v.1.43q software [23] to obtain the average particle size and shape factor S . Shape factor is a measure of the circularity of a particle and is calculated as follows:

$$S = \frac{4\pi A}{C^2} \quad (2)$$

where A is the particle area and C is the particle circumference. The values for the shape factor lie in the range of $0 \leq S \leq 1$, where $S = 1$ corresponds to a circular object [13].

The structure of the nanocomposite coatings deposited on the monofilament polyethylene terephthalate (PET) fibres was visualized by an S-4800 scanning electron microscope (SEM) (Hitachi, Japan) at an accelerating voltage of 1kV and an 11μA emission current. Samples were scanned as prepared, i.e., without any additional metal over-coating.

The electrical properties of the deposited nanocomposite films were characterized using a Keithley 6430 Sensitive SourceMeter (Keithley, USA) by a 2-point probe method in a range from -1V to +1V. For this purpose, films were deposited on planar glass slides (Assistent, Germany) as well as monofilament PET fibres with pre-deposited segmented silver electrodes. In this configuration, the current flow was along the plane of the film. From the obtained I-V curves, the resistance R was determined by linear regression analysis using the "least squares" method. Finally, a sheet resistance R_{SH} was calculated using Equation (3) to be able to compare results from samples with different geometries:

$$R = \frac{\rho}{t} \cdot \frac{L}{W} = R_{SH} \cdot \frac{L}{W} \quad (3),$$

where ρ is the bulk resistivity of the nanocomposite material, t is the thickness of the nanocomposite film, L is the length of the sample (i.e., the separation of the respective electrodes) and W is the width of the sample (i.e., the length of the electrode).

The thickness of the studied nanocomposite films deposited on glass substrates was measured directly by a surface profiler Dektak 150 (Veeco, USA) along film edges at 6 different positions on the film surface. Measurement error was estimated to be 10% resulting mainly from the thickness uniformity of the deposited coatings. The thickness of films deposited on carbon foils used for TEM characterization and films deposited on PET fibres was estimated from the deposition rates measured separately. Measurement error was estimated to be 15% in this case.

Where applicable, the films were characterized as-prepared directly after the deposition and then were

stored in a box in ambient conditions (20°C and 40% relative humidity) for ageing. The films were then characterized again after 1 month for comparison. For the study of the influence of an aqueous environment on the nanocomposite films, selected films were characterized before and after immersion into water for either 1 hour (coatings on glass substrates) or 30 seconds (coatings on fibres). After the water incubation, prior to the characterization, any remaining water droplets were soaked away from the surface of the samples.

3. Results and discussion

3.1 In-situ characterization of plasma discharge by OES

Plasma discharge composition was monitored during the deposition of Ag/a-C:H:O nanocomposite films using *in-situ* OES. A typical spectrum recorded at an RF discharge power of 50W is presented in Figure 2, with corresponding identification of the emitting species.

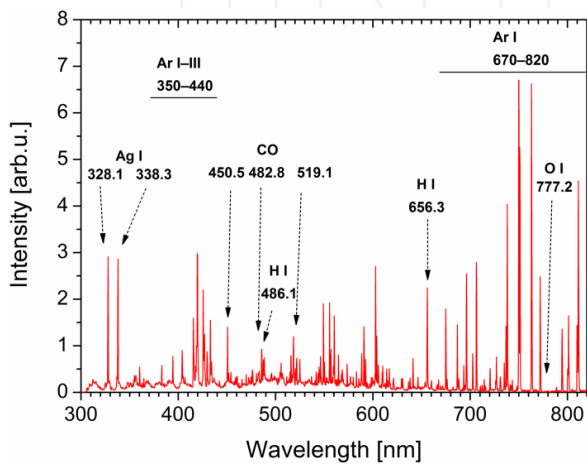


Figure 2. OES of glow discharge during sputtering of Ag in Ar/CO₂/C₂H₄ atmosphere at RF power of 50W. Identified emitting species are listed together with their respective wavelengths in [nm].

The most important part of the spectrum for our analysis is a region at shorter wavelengths (300–450nm), which comprises the atomic emission lines of silver species (²P_{3/2} at 328.1nm and ²P_{1/2} at 338.3nm) originating from excited states after sputtering from the target. The intensity of the emission line of Ag is proportional to the sputtering rate and thus also a measure of the deposition rate of Ag from the sputtering target [24, 25]. Therefore, monitoring the level of intensity of one or both of the emission lines of silver is a convenient means for controlling the deposition rate of silver, which is a factor determining the final filling factor. A fine control is important for the preparation of films near the percolation threshold, which requires enhanced stability of deposition conditions. Further, this spectral region also contains relatively intensive atomic emission lines of argon species, namely between 350nm and 440nm. The central part of the emission spectrum contains various bands of CO radicals

(450.5nm, 482.8nm and 519.1nm) together with atomic emission lines of hydrogen (486.1nm and 656.3nm). Finally, the region of longer wavelengths above 670nm is dominated by strong atomic emission lines of various argon species. Only traces of atomic oxygen were detected at 777.2nm.

3.2 Microstructure of nanocomposite films

As has already been mentioned, the microstructure of nanocomposite films plays a decisive role in determining the electrical properties of Ag/a-C:H:O coatings. The dependence of the filling factor on the applied RF power in a range from 50W to 100W is represented in Figure 3. Filling factors are determined using ICP-OES as previously described. It can be observed that the amount of silver in the nanocomposite films increases with the RF power applied. This is caused by the fact that the sputtering rate of silver atoms increases more rapidly with applied power than the plasma polymer deposition rate, resulting in a higher metal content within the Ag/a-C:H:O nanocomposites.

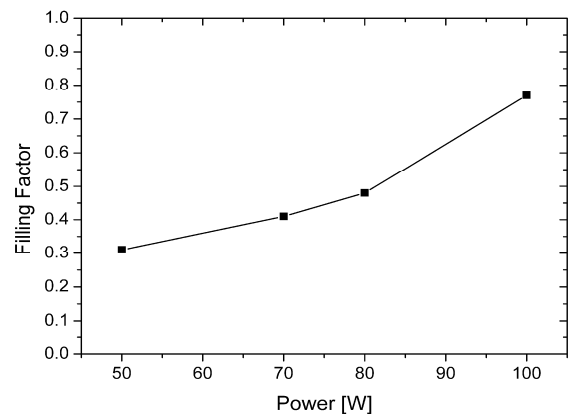


Figure 3. Dependence of filling factor on the RF power applied during deposition of Ag/a-C:H:O nanocomposite coatings.

According to several literature sources, the percolation threshold f_c lies slightly below a filling factor of 0.5, particularly for Ag/C:H composite films. Biederman estimated the f_c to lie between 0.3 and 0.4 [10], while Heilmann set it to 0.3 [13]. In the case of our deposition conditions, the most favourable RF power for preparation of Ag/a-C:H:O nanocomposite films with a structure close to percolation threshold would be around 50W. This means that the processes at an RF power lower than 50W would result in films with high electrical resistance, while the electrical resistance of films deposited at powers higher than 50W would be low enough for signal conduction. The filling factors around the threshold were confirmed by a thorough TEM characterization of the coatings prepared under various RF powers in the range of 20W to 80W. This data is intended for publication in a separate communication. To this end, we concentrate on the characterization of the properties the Ag/a-C:H:O nanocomposite films prepared at RF power of 50W.

TEM micrographs at various magnifications and a matching electron diffraction pattern of Ag/a-C:H:O nanocomposite film with thickness $(20\pm 3)\text{nm}$ were prepared at an RF power of 50W as displayed in Figure 4. It can be seen that silver nanoparticles (dark areas) are randomly distributed in the plasma polymer matrix (brighter areas). Under higher magnification, it can be seen that the metal nanoparticles contact each other at multiple locations. This is the basis for the percolation path through which electrical current can travel in an extended particle network through the nanocomposite. The film finally becomes an electrical conductor in which the mean free path for electrons is in order of several tens of nanometres (e.g., 23.6nm for gold thin film [13]). SAD analysis indicates that the crystal structure of the silver nanoparticles is cubic centrosymmetric [22]. The diffraction planes with orientations (111), (002), (022), (113) and (024) were also identified.

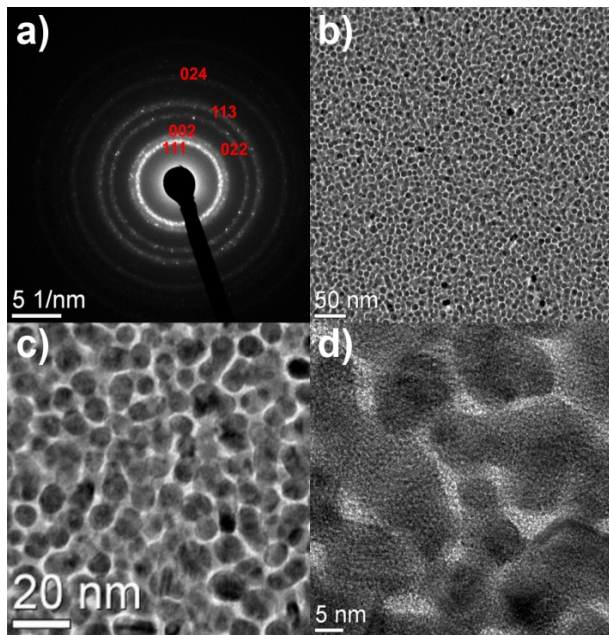


Figure 4. Diffraction pattern with respective Miller indices (a) and TEM micrographs of Ag/a-C:H:O nanocomposite film (thickness 20nm) prepared at RF power of 50W at various magnifications: b) $\times 50,000$, c) $\times 100,000$ and d) $\times 400,000$.

Statistical evaluation of TEM micrographs revealed that the average size of metal nanoparticles is about 9nm with rather narrow size distribution (standard deviation $\sigma = 1\text{nm}$) (see Figure 5). Most of the nanoparticle diameters are between 7nm and 12nm. On the other hand, the distribution of the shapes of the nanoparticles is very broad (standard deviation $\sigma = 0.18$) which suggests a percolation structure of the nanocomposite. Nevertheless, most of them are almost circular ($S = 0.85$) even though the shape factor values range from 0.15 to 0.95.

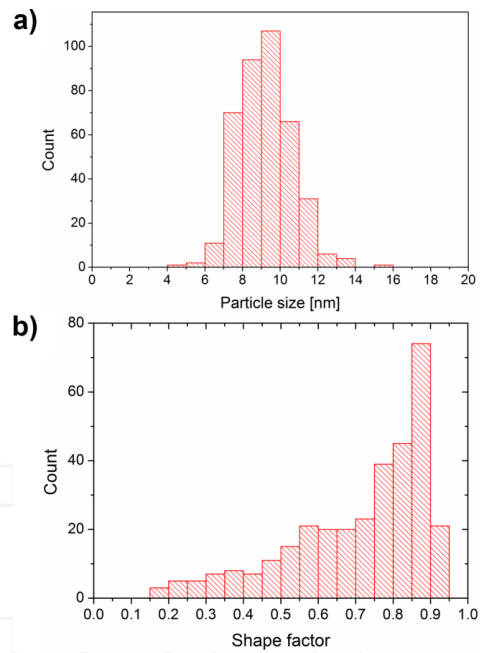


Figure 5. Statistical distribution of a) size and b) shape of silver nanoparticles in Ag/a-C:H:O nanocomposite film prepared at RF power of 50W.

3.3 Electrical properties of nanocomposite films

The electrical properties of Ag/a-C:H:O nanocomposite films prepared at various RF powers were at first characterized on plane glass substrates. The obtained I-V curves reveal overall linear Ohmic characteristics for all of the films, as can be seen from the example of nanocomposite film prepared at an RF power of 50W in Figure 6. The linear characteristics of films prepared at different powers differ in the slope of the dependence, i.e., resistivity of the coatings. The electrical properties correlate with the TEM characterization of the microstructure; it showed that films prepared at 50W possess a structure at the percolation threshold.

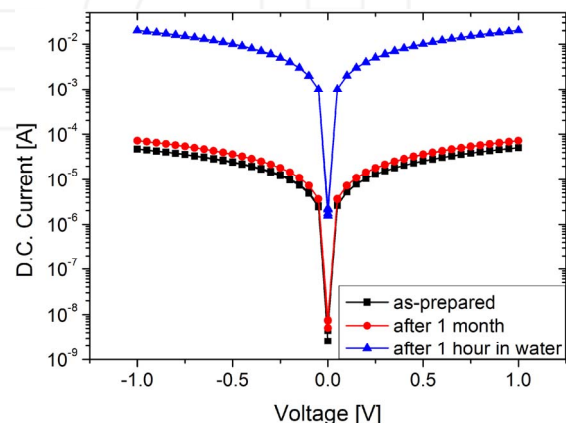


Figure 6. I-V characteristics of Ag/a-C:H:O nanocomposite film (thickness 20nm) deposited at RF power of 50W on a plane glass substrate: as prepared, 1 month after the deposition and as-prepared after immersion into water for 1 hour.

To assess the stability of this sensor layer, we also characterized samples: i) after 1 month of ageing and ii) after 1 hour incubation in water. As documented in Figure 6 and Table 1, only minor differences in the I-V curves and in the values of R_{SH} were observed between the as-prepared and 1-month-old nanocomposite coatings. The sheet resistance of as-prepared films was $6.0 \cdot 10^4 \Omega/\text{sq}$, while it was $4.0 \cdot 10^4 \Omega/\text{sq}$ for the aged films. Since the total measurement error is about 10%, we can expect that some small changes in the microstructure of the nanocomposite coatings might occur over time, e.g., atom diffusion or recrystallization [13,26]. However, Biederman et al. previously reported distinct changes in the microstructure of Ag/C:H nanocomposite films on a time scale of several days [27]. Such substantial changes were not observed here with Ag/a-C:H:O films. In contrast, the changes in the resistivity of the coatings after being in contact with aqueous environment are several orders of magnitude (see Figure 6 and Table 1). Particularly, the resistivity of the coating immersed into a water bath for 1 hour decreased to $2.0 \cdot 10^2 \Omega/\text{sq}$.

Several different processes might take place during a contact of Ag/a-C:H:O nanocomposite films with an aqueous environment. These might influence the structure of the films yielding a change in their electrical properties. Some of them might cause an increase in resistivity of the coatings, especially due to the disruption of the percolation structure (e.g., swelling of the plasma polymer matrix, leaching of Ag^+ ions and various microstructural changes like recrystallization or coalescence) [16, 28]. However, these effects appear to be minor, since the observed decrease in the resistivity rather suggests an enhanced percolation network or a decrease of inter-particle contact resistance. These are likely to be caused by water penetration into the hydrophilic plasma polymer matrix and/or its adsorption onto Ag nanoparticles, thus improving the percolation pathway for electrical conduction. These effects can remain even after removal from the water bath. However, the direct cause of the observed phenomenon is not known exactly and therefore, further research is being conducted in this direction.

3.4 Nanocomposite film on a fibre

We also transferred Ag/a-C:H:O nanocomposite films onto monofilament PET textile fibres with previously patterned silver electrodes utilizing a specially designed structured masking system. Examples of a fibre with deposited structured silver electrodes and a fibre coated by Ag/a-C:H:O nanocomposite film are illustrated in Figure 7. As seen in Figure 7b, the structured silver electrode is not sharply terminated. This is a minor flaw of the masking system used here (a new system was later developed). We verified that the transition zone did not have any measurable effect on the electrical

characterization. The nanocomposite films are deposited with very low roughness and no defects were observed on the surface of the coatings (Figure 7c). This straightforward transfer onto the fibre geometry is remarkable.

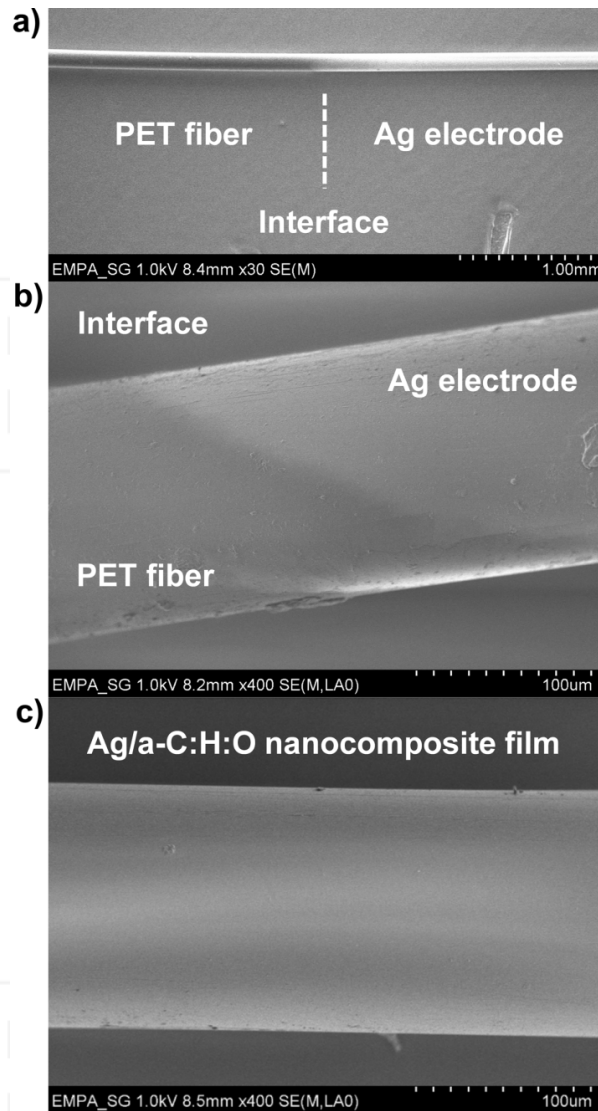


Figure 7. SEM images of PET fibre coated with silver thin film electrode (thickness 60nm) at magnification a) x30 and b) x400 and c) Ag/a-C:H:O nanocomposite film (thickness 20nm) prepared at RF power of 50W (magnification x400).

The I-V curves of the Ag/a-C:H:O nanocomposite film deposited at an RF power of 50W on a PET monofilament fibre can be seen in Figure 8. Similarly to the films deposited on reference glass substrates, the films on the fibres also reveal linear Ohmic characteristics, which differ only in the slopes of the I-V curves (on a linear plot). The sheet resistance R_{SH} was about $6.7 \cdot 10^6 \Omega/\text{sq}$. This is two orders of magnitude higher than the planar film on the glass substrate (see Table 1). We think this effect is due to a change in the polymer matrix properties induced by the different substrate and masking geometry in the plasma. Also, the structure of coatings deposited

on glass substrates and PET fibres might differ slightly due to different surface diffusion coefficients. There might be a small deviation from the percolation structure in the films deposited on PET fibres since it is extremely sensitive to the experimental conditions. A more detailed analysis is underway to clarify this point.

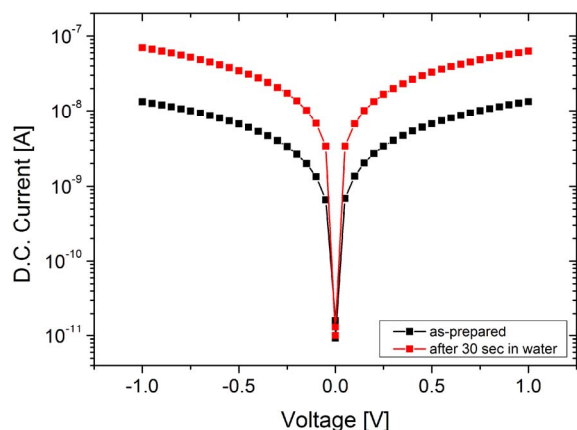


Figure 8. I-V characteristics of Ag/a-C:H:O nanocomposite film (thickness 20nm) deposited at RF power of 50W on a PET fibre, as measured right after the deposition and after immersion into water for 30 seconds.

As in the planar films, the resistivity decreases significantly after contact with water and subsequent drying. The effect is however less strong; the R_{SH} of a film deposited on the fibre at 50W and put into water for 30 seconds was measured to be $1.4 \cdot 10^6 \Omega/\text{sq}$ (Table 1). Again, this difference in wetting behaviour suggests that the polymer matrix has different properties in the fibre geometry. We think a higher ion bombardment in the presence of the fibre masking system results in the growth of a denser and a more cross-linked plasma polymer matrix.

Thin film	$R_{SH} [\Omega/\text{sq}]$
as-prepared on plane glass	$6.0 \cdot 10^4$
after 1 month on plane glass	$4.0 \cdot 10^4$
after 1 hour in water on plane glass	$2.0 \cdot 10^2$
as-prepared on fibre	$6.7 \cdot 10^6$
after 30 sec in water on fibre	$1.4 \cdot 10^6$

Table 1. Calculated sheet resistances R_{SH} of Ag/a-C:H:O nanocomposite films.

4. Conclusions

This study showed that Ag/a-C:H:O nanocomposite films prepared by simultaneous plasma polymerization of ethene and sputtering of a silver target possess sensor functionality in aqueous and humid environments. We demonstrated their successful deposition on monofilament PET fibres, where the sensor properties remained intact. This is a first step towards sensing in smart textiles. The deposition process was monitored through *in-situ* OES, which allows online controlling of

the process stability. The filling factor and particle statistics of the Ag/a-C:H:O nanocomposite films were characterized by ICP-OES and TEM, respectively. We showed that planar coatings with structure at percolation threshold are deposited at RF power of 50W in our vacuum deposition chamber. The films revealed only minor changes of the properties upon ageing in air. Additional work is on going to further elucidate the details of the conduction mechanisms and history effects. Such sensor coatings may form the basis for future smart textiles or low cost humidity/water history recording devices.

5. Acknowledgments

Financial support from the Sciex-NMSch programme under project 10.118 – ExTraSens and from the Swiss National Funding (SNF) within the project NanoTera (Tec-in-Tex) is acknowledged. The authors would also like to acknowledge Elisabeth Michel, Empa, St. Gallen, for performing the ICP-OES measurements and Leonie El Issawi-Frischknecht, Empa, St. Gallen, for performing the SEM characterization.

6. References

- [1] Chen Z, Lu C (2005) Humidity sensors: A review of materials and mechanisms. *Sensor Lett.* 3: 274-295.
- [2] Kulwicki B.M (1991) Humidity sensors. *J. Am. Ceram. Soc.* 74: 697-708.
- [3] Sakai I, Sadaoka Y, Matsaguchi M (1996) Humidity sensors based on polymer thin films. *Sens. Actuators B.* 35-36: 85-89.
- [4] Tröster G (2004) The Agenda of Wearable Healthcare. In: Haux R, Kulikowski C, editors. *IMIA Yearbook of Medical Informatics 2005*. Stuttgart: Schattauer. 125-138.
- [5] Biederman H, Osada Y (1992) *Plasma Polymerization Processes*. Amsterdam: Elsevier.
- [6] Faupel F, Zaporajtchenko V, Strunskus T, Elbahri M (2010) Metal-polymer nanocomposites for functional applications. *Adv. Eng. Mater.* 12: 1177-1190.
- [7] Biederman H, Kylian O, Drabik M, Choukourov A, Polonskyi O, Solar P (2012) Nanocomposite and nanostructured films with plasma polymer matrix. *Surf. Coat. Tech.* 211: 127-137.
- [8] Hanisch C, Ni N, Kulkarni A, Zaporajtchenko V, Strunskus T, Faupel F (2011) Fast electrical response to volatile organic compounds of 2D Au nanoparticle layers embedded into polymers. *J. Mater. Sci.* 46: 438-445.
- [9] Drabik M, Hanus J, Kousal J, Choukourov A, Biederman H, Slavinska D, Mackova A, Pesicka J (2007) Composite TiO_x/Hydrocarbon Plasma Polymer Films Prepared by Magnetron Sputtering of TiO₂ and Poly(propylene). *Plasma Process. Polym.* 4: 654-663.

- [10] Biederman H (2004) Plasma Polymer Films. London: Imperial College Press.
- [11] Hrach R, Novak S, Svec M (2006) Correlation between morphology and transport properties of composite films: Charge transport in composites. *Appl. Surf. Sci.* 252: 5516–5520.
- [12] Laurent C, Kay E (1989) Properties of metal clusters in polymerized hydrocarbon versus fluorocarbon matrices. *J. Appl. Phys.* 65: 1717-1723.
- [13] Heilmann A (2003) Polymer films with embedded metal nanoparticles. Berlin: Springer.
- [14] Kay E (1986) Synthesis and Properties of Metal Clusters in Polymeric Matrices. *Z. Phys. D - Atoms, Molecules and Clusters.* 3: 251-262.
- [15] d'Agostino R (1990) Plasma Deposition, Treatment and Etching of Polymers. New York: Academic Press.
- [16] Körner E, Aguirre M.H, Fortunato G, Ritter A, Rühle J, Hegemann D (2010) Formation and distribution of silver nanoparticles in a functional plasma polymer matrix and related Ag⁺ release properties. *Plasma Process. Polym.* 7: 619-625.
- [17] Amberg M, Kasdallah C, Ritter A, Hegemann D (2010) Influence of Residual Oils on the Adhesion of Metal Coatings to Textiles. *J. Adhes. Sci. Technol.* 24: 123-134.
- [18] Amberg M, Grieder K, Barbadoro P, Heuberger M, Hegemann D (2008) Electromechanical Behavior of Nanoscale Silver Coatings on PET Fibers. *Plasma Process. Polym.* 5: 874-880.
- [19] Körner E, Fortunato G, Hegemann D (2009) Influence of RF Plasma Reactor Setup on Carboxylated Hydrocarbon Coatings. *Plasma Process. Polym.* 6: 119-125.
- [20] National Institute of Standards and Technology, Atomic Spectra Database, http://physics.nist.gov/PhysRefData/ASD/lines_form.html (accessed September 2012).
- [21] Drabik M, Serov A, Kylian O, Choukourov A, Artemenko A, Kousal J, Polonskyi O, Biederman H (2012) Deposition of Fluorocarbon Nanoclusters by Gas Aggregation Cluster Source. *Plasma Process. Polym.* 9: 390-397.
- [22] The International Centre for Diffraction Data, Powder Diffraction File, <http://www.icdd.com/>.
- [23] Rasband W, National Institute of Health, USA, ImageJ project, image processing program, <http://rsb.info.nih.gov/ij/>.
- [24] Biederman H, Chmel Z, Fejfar A, Misina M, Pesicka J (1990) Temperature induced structural rearrangements of Ag/a-C: H composite films and their dc electrical conduction. *Vacuum.* 40: 377-380.
- [25] Hanus J, Drabik M, Hlidek P, Biederman H, Radnoczi G, Slavinska D (2009) Some remarks on Ag/C:H nanocomposite films. *Vacuum* 83: 454–456.
- [26] Faupel F, Willecke R, Thran A (1998) Diffusion of metals in polymers. *Mat. Sci. Eng. R22:* 1-55.
- [27] Biederman H, Hlidek P, Pesicka J, Slavinska D, Stundzia V (1996) Deposition of composite metal/C:H films - the basic properties of Ag/C:H. *Vacuum.* 47: 1385-1389.
- [28] Liu J, Hurt R.H (2010) Ion Release Kinetics and Particle Persistence in Aqueous Nano-Silver Colloids. *Environ. Sci. Technol.* 44: 2169-2175.

INTECH